ACS Photonics

Article

pubs.acs.org/journal/apchd5

Chiral Nanomagnets

Sahand Eslami,[†] John G. Gibbs,[†,‡] Yvonne Rechkemmer,[§] Joris van Slageren,[§] Mariana Alarcón-Correa,[†,§] Tung-Chun Lee,[†] Andrew G. Mark,[†] Geert L. J. A. Rikken,[∥] and Peer Fischer*[,†,§]

[†]Max-Planck-Institut für Intelligente Systeme, Heisenbergstraße 3, 70569 Stuttgart, Germany

[‡]Department of Physics and Astronomy, Northern Arizona University, S. San Francisco Street, Flagstaff, Arizona 86011, United States

[§]Institut für Physikalische Chemie, Universität Stuttgart, Pfaffenwaldring 55, 70569 Stuttgart, Germany

[∥]Laboratoire National des Champs Magnétiques Intenses, UPR3228 CNRS/INSA/UJF/UPS, Toulouse and Grenoble, France

ABSTRACT: We report on the enhanced optical properties of chiral magnetic nanohelices with critical dimensions comparable to the ferromagnetic domain size. They are shown to be ferromagnetic at room temperature, have defined chirality, and exhibit large optical activity in the visible as verified by electron microscopy, superconducting quantum interference device (SQUID) magnetometry, natural circular dichroism (NCD), and magnetic circular dichroism (MCD) measurements. The structures exhibit magneto-chiral dichroism (MChD), which directly demonstrates coupling between their structural chirality and magnetism. A chiral nickel (Ni) film consisting of an array of nanohelices ~100 nm in length exhibits an MChD anisotropy factor $g_{MChD} \approx 10^{-4}$ T^{-1} at room temperature in a saturation field of ~0.2 T, permitting polarization-independent control of the film's absorption properties through magnetic field modulation. This is also the first report of MChD in a material with structural chirality on the order of the wavelength of light, and therefore the Ni nanohelix array is a metamaterial with magnetochiral properties that can be tailored through a dynamic deposition process.

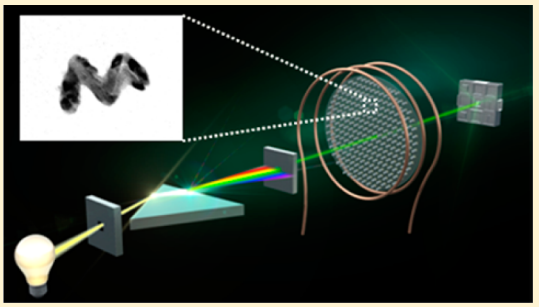

KEYWORDS: *nanomagnet, ferromagnetism, chiral, nanohelix, circular dichroism, magnetochiral dichroism*

As the critical dimensions of a magnet approach the ferromagnetic domain size, structural morphology becomes increasingly important in relation to its magnetic properties, as magnetic domain formation is suppressed.[1] For ferromagnetic nanoparticles of <100 nm, or *nanomagnets*, the domain size and the electron transport scattering length can both be of the same length scale as the size of the particles themselves. Such nanoscale magnetic materials are interesting due to possible applications as high-density data storage media or for the study of more fundamental properties such as magnetic vortex formation.[2,3]

Nanoscale materials are particularly compelling because multiple properties can arise from the same morphological confinement. For example, nickel (Ni) is ferromagnetic and Ni nanoparticles can also support surface plasmon resonances;[4−6] therefore, a geometric constraint in nanoscale Ni not only limits the formation of multiple ferromagnetic domains but can also lead to localized surface plasmon resonance (LSPR). Since the properties of a nanomagnet are highly geometry dependent, structural asymmetries can be expected to induce corresponding asymmetries in its properties as well.

Herein, we report experiments that reveal the direct coupling of magnetic and optical properties of chiral Ni nanomagnets. To the best of our knowledge, the structures in this article are the smallest magnetic nanohelices that have been realized to date. They interact strongly with visible light, and we show that the optical response can be modulated with an external magnetic field. In particular, the coupling of the nanoparticle chirality to the field, i.e., the simultaneous absence of parity and time reversal symmetry, leads to a higher order optical response termed magnetochiral dichroism (MChD),[7] which manifests itself as a magnetic-field-tunable, polarization-independent absorption effect.

MAGNETOCHIRAL DICHROISM

When a nanomaterial is chiral and on the order of the wavelength of visible light, it will interact differently with the two circular polarization (CP) states of light, which are themselves chiral.[8−18] In particular, isotropic chiral media exhibit natural circular dichroism (NCD), absorbing one CP state more than the other, which causes an impinging beam of linearly polarized light to become elliptically polarized. Similarly, any medium in the presence of a magnetic field (parallel to the direction of light propagation) will also show differential absorption proportional to the field strength, i.e., magnetic circular dichroism (MCD). The former is mediated by the imaginary component of the product of an electric-dipolar−magnetic-dipolar transition moment, whereas the latter is a function of a product of two electric-dipolar and one magnetic-dipolar transition moments. Whereas NCD is dependent upon the chirality of the medium, MCD (and

Received: August 18, 2014
Published: October 16, 2014

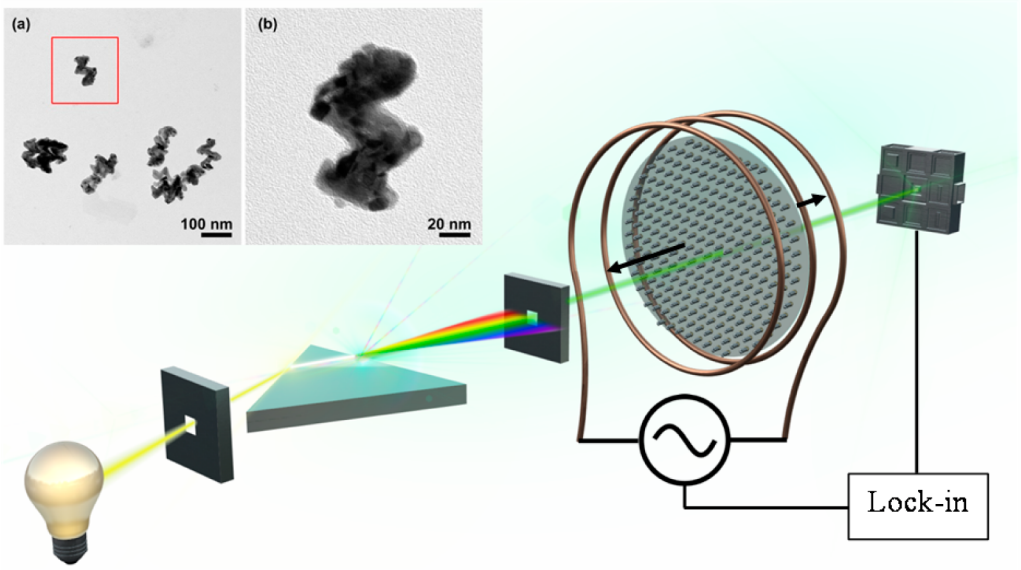

Figure 1. Schematic of the experimental setup to measure magnetochiral dichroism. An alternating current in the coil produces an alternating magnetic field that is either parallel or antiparallel with the monochromatic incident beam. The transmitted light is phase sensitively detected at the frequency of the magnetic field, and the difference in absorbance of unpolarized light is recorded on a computer (not shown). Inset: (a) Group of Ni nanohelices imaged on a TEM grid after they have been removed from the surface; (b) zoomed-in TEM image of the nanohelix shown in the box of (a).

Faraday rotation in general) is not. These effects can be summarized by expanding the generalized dielectric function ϵ in the presence of a magnetic field for left (LH) and right (RH) handed media in terms of the wavevector $\mathbf{k}$ and external magnetic field $\mathbf{B}$,[19]

$$\epsilon_{\pm}^{L/R}(\omega, \mathbf{k}, \mathbf{B}) = \epsilon(\omega) \pm \alpha^{L/R}(\omega)\mathrm{k} \pm \beta(\omega)B + \gamma^{L/R}(\omega)\mathbf{k}\cdot\mathbf{B} + \ldots \quad (1)$$

in which +/− indicate LCP and RCP, respectively, α describes the ($\mathbf{B} = 0$) natural optical activity tensor and NCD, and β is the electric-electric−magnetic-dipolar tensor that underlies the Faraday effect and MCD. The cross-term, γ, characterizes the additional effect of a magnetic field in the presence of a chiral medium, and it depends on the chiral sense and the relative orientation of $\mathbf{k}$ and $\mathbf{B}$, but not on the polarization of the light. It manifests itself in absorption as magnetochiral dichroism, which has been previously observed in chiral crystals and molecules.[7,20−22] The tensors α and γ are nonzero only if the medium is chiral and change sign with the handedness of the enantiomorph. Because MChD is a cross-term, it is expected to be strong in systems that show substantial NCD and MCD.[23] In ferromagnetic, plasmonic nanohelices both NCD and MCD should be enhanced, thus giving large values for MChD.

The schematic for the measurement of the effect is shown in Figure 1. The sample is placed in an alternating magnetic field generated by a solenoid. The sample is arranged so that the wavevector is perpendicular to the sample surface and therefore parallel to the helix and optical axes. Depolarized visible light, with wavelengths selected by a monochromator, passes through the sample while the external magnetic field is either parallel or antiparallel to the propagation direction of the light field. The magnitude of the absorbance of unpolarized light is a function of the field strength and the magnetic field direction and changes sign with the handedness of the nanohelices (the enantiomorphs).

FABRICATION

We have recently shown that glancing angle deposition (GLAD)[24−26] in conjunction with micelle nanolithography and substrate cooling may be used to grow helix structures with feature sizes less than 20 nm and overall dimensions that are a fraction of the wavelength of visible light.[27,28] We note that GLAD has also recently been used to construct nanoscale cobalt[29] and iron helices[30] of larger dimensions. Here, we grow ∼100 nm, two-turn Ni nanohelices on seeded glass substrates patterned by block copolymer micelle lithography (BCML),[31] where the optical resonances can be easily tailored by altering the deposition process, as we have recently shown.[32] The seeds upon which the helices grow are hexagonally arranged gold nanoparticles of 15 nm diameter at a mean 75 nm separation. The deposition was performed at room temperature using electron-beam evaporation at a pressure $\sim 5 \times 10^{-6}$ mbar, with a fixed tilt angle $\alpha = 85°$. From the electron microscopy images, we conclude from a qualitative standpoint that the structures have adequate fidelity when fabricated at room temperature, but we expect lower temperatures to improve structure by suppressing diffusion. The azimuthal rotation angle of the substrate holder was controlled in real time based on the thickness reading of a quartz crystal monitor, which measured a deposition rate of $\sim 4 \times 10^{-2}$ nm/s.

The resulting arrays of Ni nanohelices are shown in the inset transmission electron microscopy (TEM) images of Figure 1 and the high-angle annular dark field scanning transmission electron microscopy (HAADF STEM) images of Figure 2 (both off wafer). The image in Figure 2 shows the elemental makeup of the structure: the majority is Ni, as expected, while the Au seed and the Ti adhesion layer can be resolved as well. The rotation sense of the substrate during deposition fixes the sample chirality, and the two enantiomeric forms, i.e., LH and RH, can be seen in the Figure 3 inset showing cross-section scanning electron microscopy images (SEM) on the wafer, respectively. The total height is ∼100 nm, with two turns giving a helix pitch of ∼50 nm. A continuous (unstructured) Ni thin

dx.doi.org/10.1021/ph500305z | ACS Photonics 2014, 1, 1231−1236

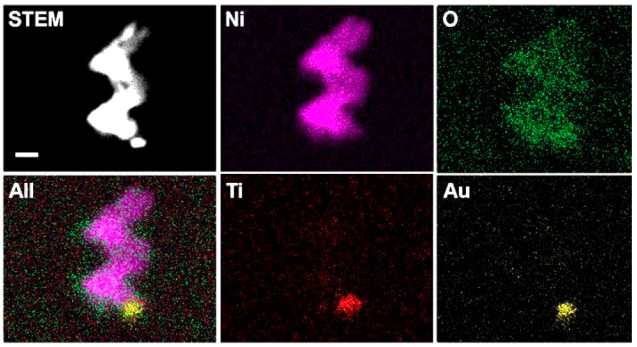

Figure 2. High-angle annular dark field scanning transmission electron microscopy (HAADF STEM) image (top left) of a typical nickel nanohelix and the corresponding false-color elemental maps obtained by STEM-EDX spectral mapping, confirming all the intended elemental constituents within the nanostructure. Scale bar = 20 nm.

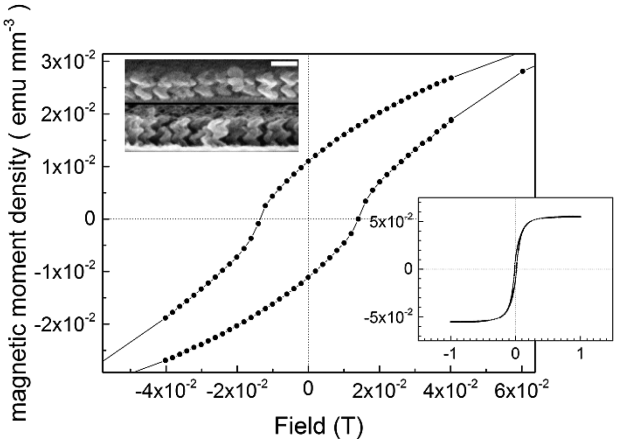

Figure 3. Magnetization curve measured parallel to the axis of the left-handed nanohelices measured with a SQUID magnetometer. The bottom-right inset shows the wide field magnetization curve with saturation at ~0.2 T. The top-left inset shows cross-section SEM images of the two-turn, ~50 nm pitch Ni nanohelices of type LH on top and RH on bottom. Scale bar = 100 nm.

film of the same thickness was grown under perpendicular incidence ($\alpha = 0°$) as an achiral control sample.

MAGNETIC PROPERTIES

We expect that a nanohelix that retains its magnetism will give a stronger MCD response than a paramagnetic one, and here we show that the helix arrays are indeed ferromagnetic. The magnetic properties are characterized using superconducting quantum interference device (SQUID) magnetometry at room temperature. A static magnetic field is applied, and the magnetization is measured along the normal and in-plane directions (not shown here), i.e., parallel and perpendicular to the helix axis. Figure 3 shows the magnetization measurements along the axes, and the curve shows ferromagnetic hysteresis. We observe for both LH and RH films a saturation field of 0.2 T, a saturation magnetization of 5×10^{-2} emu mm^{-3}, and a coercive field of 140 G. The dimensions of an individual Ni structure are on the same order as the superparamagnetic domain size, which leads to long, but finite, Néel relaxation times. Measurements of the remnant magnetization relaxation time, $\tau \approx 1.5 \times 10^3$ s, suggest that the structures have a mean magnetic domain size of 18 nm according to the Néel–Arrhenius model.[33] This agrees well with the measured helical wire diameter of ~20 nm. In contrast to recent reports on cobalt helices,[29] we do not observe effects due to the magnetic coupling between individual particles.

OPTICAL MEASUREMENTS AND RESULTS

Since MChD can be considered a cross-effect between natural circular dichroism and magnetic circular dichroism, we first measure the NCD and MCD spectra. In general, circular dichroism (CD) is defined as the differential absorption between left and right circularly polarized light: CD = $A_- - A_+$ where A_- and A_+ are the absorbances for LCP and RCP, respectively. We measure in the absence of a magnetic field the natural circular dichroism of the chiral film, NCD = CD($\mathbf{B} = 0$), and then the purely magnetic contribution to magnetic circular dichroism, MCD = CD($\mathbf{B}$) − NCD. The combination effect of natural and magnetic optical activity is determined by measuring the magnetochiral dichroism, MChD = $A(\mathbf{k} \uparrow\uparrow \mathbf{B}) - A(\mathbf{k} \uparrow\downarrow \mathbf{B})$, where $A = (A_- + A_+)/2$ is the absorbance of unpolarized light and $\mathbf{k} \uparrow\uparrow \mathbf{B}$ and $\mathbf{k} \uparrow\downarrow \mathbf{B}$, refer to parallel and antiparallel arrangements of the $\mathbf{B}$ and $\mathbf{k}$ vectors, respectively. We also compute the respective anisotropy factors for all three effects, which normalize the measurements to the total absorbance, defined as

$$g_{\mathrm{NCD}} = \frac{\mathrm{NCD}}{A(\mathbf{B}=0)}, \quad g_{\mathrm{MCD}} = \frac{\partial}{\partial B}\frac{\mathrm{MCD}}{A(\mathbf{B}=0)}, \quad g_{\mathrm{MChD}} = \frac{\partial}{\partial B}\frac{\mathrm{MChD}}{A(\mathbf{B}=0)} \tag{2}$$

We examine three samples: LH (left-handed) and RH (right-handed) nanohelices as well as achiral control films of Ni with the same nominal thickness (i.e., 100 nm). The total absorbance of each sample, $A(\mathbf{B} = 0)$, necessary for calculating the g factors was measured in transmission for unpolarized light using a Cary 4000 UV–vis spectrometer, and the NCD measurements were carried out on a JASCO 810C spectropolarimeter. Figure 4 shows the NCD spectra of the LH and RH samples in the visible region where the plasmonic resonance of Ni leads to an enhanced signal showing a large CD. Expressed in the conventional units of ellipticity, $\tan\theta = (E_R - E_L)/(E_R + E_L)$, where E_R and E_L are the magnitudes of the electric field for RCP and LCP, respectively. The 100 nm

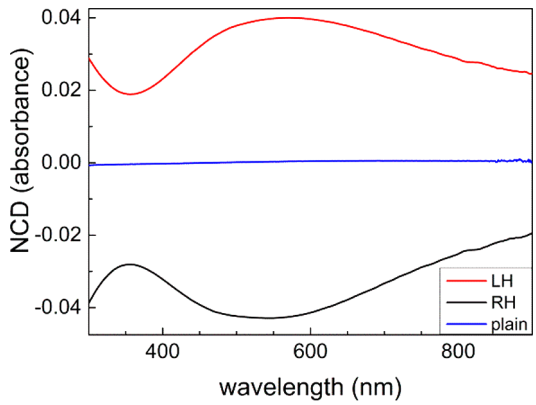

Figure 4. Natural circular dichroism spectra recorded under normal incidence on structured LH (red, top) and RH (black, bottom) two-turn Ni nanohelices. An unstructured plain Ni film is shown as a control and shows no NCD, as expected.

dx.doi.org/10.1021/ph500305z | ACS Photonics 2014, 1, 1231–1236

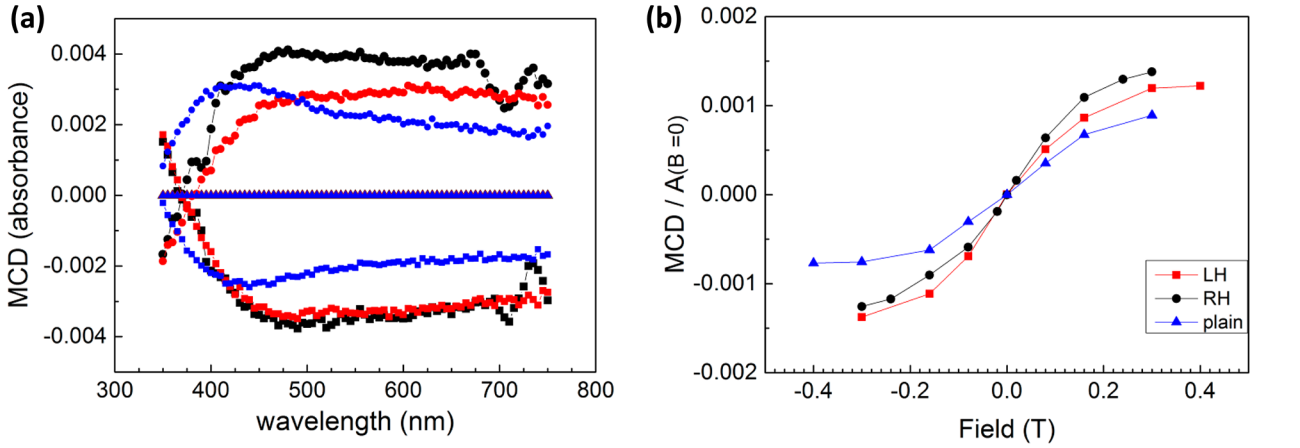

Figure 5. (a) MCD of unstructured plain film (blue) and LH (red) and RH (black) Ni nanohelices at −0.3 T (squares), 0.0 T (triangles), and +0.3 T (circles), respectively. (b) Magnetic field dependence of the MCD asymmetry factor (g_{MCD}) at 500 nm. Saturation of the MCD occurs for all the samples at **B** > 0.2 T.

film has an ellipticity of ∼1.3° at 550 nm. As expected, the two enantiomers give spectra of opposite sign, and the unstructured Ni film exhibits no NCD (see Figure 4).

MCD measurements were performed by recording spectra on an AVIV 42 MCD spectrometer coupled to an Oxford Instruments Spectromag SM4000-10, which provides magnetic fields from −10 T to +10 T. The temperature of each sample was held at 300 K. Figure 5a shows the MCD measurements in the presence of a static magnetic field **B** = ±0.3 T. Since MCD does not distinguish between the handedness of the samples, the LH and RH helices give the same MCD spectra, as expected. Although structural differences can account for small spectral differences for MCD in Figure 5(a), it is unclear why the spectra for the LH sample are asymmetric for the two measurements at B = −0.3 T and B = +0.3 T, whereas the unstructured thin film and the RH sample are symmetric. The anisotropy factor g_{MCD} measured for a single wavelength, λ = 500 nm, is shown as a function of magnetic field strength in Figure 5b. The graph shows that the value of the magnetic field at which the MCD saturates (|**B**| = 0.2 T) agrees well with that found in the magnetization measurements in Figure 3.

The MChD measurement setup is schematically shown in Figure 1. Light from the spectrometer was depolarized with an optical fiber (not shown) and guided to the sample. A custom coil pair generated magnetic fields of up to 0.2 T at 10 Hz. A second fiber-optic bundle collected the light and directed it to a photomultiplier tube (PMT) whose output was phase-sensitively recorded by a lock-in amplifier locked to the coil excitation frequency. The transmission of the unpolarized light through the sample was measured as a function of the applied magnetic field amplitude at wavelengths between 300 and 800 nm.

The results of the measurements are given in Figure 6, showing the anisotropy factor due to MChD. No detailed theory exists to model magneto-chiral anisotropy on metallic helices at optical frequencies, and existing models for low frequencies on metallic helices[34] or for free electrons on a helix[35] cannot account for the experimentally observed spectra. Yet to first-order, the dissymmetry factor for MChD is related to the dissymmetry factors for NCD and MCD by $g_{MChD} \approx {}^1/_2 g_{NCD} g_{MCD}$,[19] which is shown also in Figure 6 by the solid dots (for a magnetic field of 0.16 T). As has been observed previously,[20] the observed line shape differs from the shape

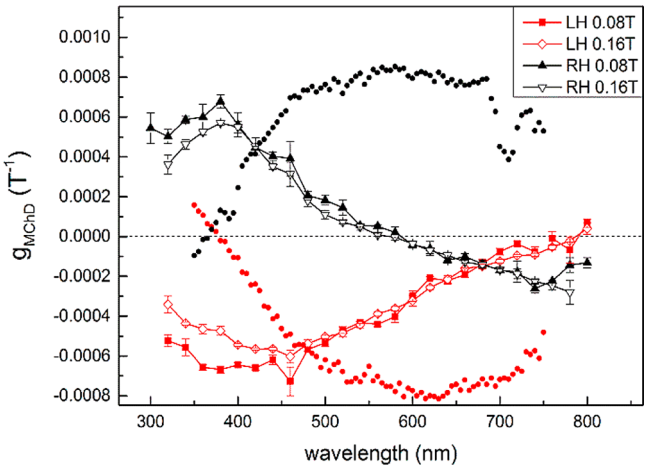

Figure 6. Magnetochiral dichroism of LH (red symbols and lines on the bottom for short wavelengths) and RH (black symbols and lines on top) nanohelix arrays at magnetic field strengths of 0.08 and 0.16 T. The scattered circles correspond to the first-order approximation of MChD based upon NCD and MCD measurements at 0.16 T.

predicted by the product, which suggests that pure MChD is the dominant contribution rather than cascaded effects. In the linear regime, we observe a slope of $g_{MChD} = (6.8 \pm 0.3) \times 10^{-4}$ T^{-1} at 380 nm for the RH helices and $g_{MChD} = (7.3 \pm 0.7) \times 10^{-4}$ T^{-1} at 460 nm for the LH helices.

CONCLUSIONS

In summary, we have fabricated and characterized chiral Ni nanomagnets with critical dimensions that are comparable to the ferromagnetic domain size, that combine strong optical activity and ferromagnetism. We have verified that the structures are indeed ferromagnetic with SQUID magnetometry and have shown that the combination of structural chirality and magnetism gives rise to an optical response resulting from the mixing of magneto-chiral and chiroptical effects. In particular we have measured magnetochiral dichroism and shown that this effect is enhanced due to the combined ferromagnetism and structural chirality of the material. Further enhancement seems possible by incorporating more strongly ferromagnetic materials, like iron, cobalt, or samarium cobalt.

dx.doi.org/10.1021/ph500305z | ACS Photonics 2014, 1, 1231−1236

It is interesting to note that the chiral nanomagnets, due to their symmetry, should also possess a magneto-electric response. In magneto-electric media a magnetic field can influence the electric properties and vice versa, which in principle could allow for novel electronic functions, as seen in a gyrator.[36,37] Future work will focus on identifying the inverse magnetochiral anisotropy effect[38] and magnetochiral birefringence and further exploiting control over the nanomagnets' shape asymmetry to dictate their magnetization anisotropy. Combining nanoplasmonics with magnetism opens new possibilities in the control of plasmonic phenomena and devices.[39−42]

AUTHOR INFORMATION

Corresponding Author

*E-mail: fischer@is.mpg.de.

Notes

The authors declare no competing financial interest.

ACKNOWLEDGMENTS

We thank E. Goering and G. Schütz for access and support with the SQUID measurements and J. P. Spatz and C. Miksch for help with the micelle nanolithography and SEM access. We thank the Stuttgart Center for Electron Microscopy for technical support with the TEM imaging. We also thank A. Posada for assistance with the schematic. This work was in part supported by the European Research Council under the ERC Grant agreement 278213.

REFERENCES

(1) Hehn, M.; Ounadjela, K.; Bucher, J.-P.; Rousseaux, F.; Decanini, D.; Bartenlian, B.; Chappert, C. Nanoscale magnetic domains in mesoscopic magnets. *Science* **1996**, *272*, 1782−1785.

(2) Cowburn, R.; Koltsov, D.; Adeyeye, A.; Welland, M.; Tricker, D. Single-domain circular nanomagnets. *Phys. Rev. Lett.* **1999**, *83*, 1042.

(3) Shinjo, T.; Okuno, T.; Hassdorf, R.; Shigeto, K.; Ono, T. Magnetic vortex core observation in circular dots of permalloy. *Science* **2000**, *289*, 930−932.

(4) Chen, J.; Albella, P.; Pirzadeh, Z.; Alonso-González, P.; Huth, F.; Bonetti, S.; Bonanni, V.; Åkerman, J.; Nogués, J.; Vavassori, P. Plasmonic nickel nanoantennas. *Small* **2011**, *7*, 2341−2347.

(5) Halpern, A. R.; Corn, R. M. Lithographically patterned electrodeposition of gold, silver, and nickel nanoring arrays with widely tunable near-infrared plasmonic resonances. *ACS Nano* **2013**, *7*, 1755−1762.

(6) Pirzadeh, Z.; Pakizeh, T.; Miljkovic, V.; Langhammer, C.; Dmitriev, A. Plasmon−interband coupling in nickel nanoantennas. *ACS Photonics* **2014**, *1*, 158−162.

(7) Rikken, G.; Raupach, E. Observation of magneto-chiral dichroism. *Nature* **1997**, *390*, 493−494.

(8) Larsen, G. K.; He, Y.; Wang, J.; Zhao, Y. Scalable fabrication of composite Ti/Ag plasmonic helices: controlling morphology and optical activity by tailoring material properties. *Adv. Opt. Mater.* **2014**, *2*, 245−249.

(9) Schäferling, M.; Dregely, D.; Hentschel, M.; Giessen, H. Tailoring enhanced optical chirality: design principles for chiral plasmonic nanostructures. *Phys. Rev. X* **2012**, *2*, 031010.

(10) Kumar, S.; Goel, P.; Singh, D. P.; Singh, J. Highly sensitive superhydrophobic Ag nanorods array substrates for surface enhanced fluorescence studies. *Appl. Phys. Lett.* **2014**, *104*, 023107.

(11) Kuzyk, A.; Schreiber, R.; Fan, Z.; Pardatscher, G.; Roller, E.-M.; Högele, A.; Simmel, F. C.; Govorov, A. O.; Liedl, T. DNA-based self-assembly of chiral plasmonic nanostructures with tailored optical response. *Nature* **2012**, *483*, 311−314.

(12) Nair, G.; Singh, H. J.; Paria, D.; Venkatapathi, M.; Ghosh, A. Plasmonic interactions at close proximity in chiral geometries: route toward broadband chiroptical response and giant enantiomeric sensitivity. *J. Phys. Chem. C* **2014**, *118*, 4991−4997.

(13) Hentschel, M.; Schäferling, M.; Weiss, T.; Liu, N.; Giessen, H. Three-dimensional chiral plasmonic oligomers. *Nano Lett.* **2012**, *12*, 2542−2547.

(14) Larsen, G.; He, Y.; Ingram, W.; LaPaquette, E.; Wang, J.; Zhao, Y.-P. The fabrication of three-dimensional plasmonic chiral structures by dynamic shadowing growth. *Nanoscale* **2014**, *6*, 9467−9476.

(15) Schäferling, M.; Yin, X.; Engheta, N.; Giessen, H. Helical plasmonic nanostructures as prototypical chiral near-field sources. *ACS Photonics* **2014**, *1*, 530−537.

(16) Fan, Z.; Govorov, A. O. Plasmonic circular dichroism of chiral metal nanoparticle assemblies. *Nano Lett.* **2010**, *10*, 2580−2587.

(17) Fan, Z.; Govorov, A. O. Helical metal nanoparticle assemblies with defects: plasmonic chirality and circular dichroism. *J. Phys. Chem. C* **2011**, *115*, 13254−13261.

(18) McPeak, K. M.; van Engers, C. D.; Blome, M.; Park, J. H.; Burger, S.; Gosalvez, M. A.; Faridi, A.; Ries, Y.; Sahu, A.; Norris, D. J. Complex chiral colloids and surfaces via high-index off-cut silicon. *Nano Lett.* **2014**, *14*, 2934−2940.

(19) Berova, N.; Polavarapu, P. L.; Nakanishi, K.; Woody, R. W. *Comprehensive Chiroptical Spectroscopy, Applications in Stereochemical Analysis of Synthetic Compounds, Natural Products, and Biomolecules*; John Wiley & Sons, 2012; Vol. 2.

(20) Rikken, G.; Raupach, E. Pure and cascaded magnetochiral anisotropy in optical absorption. *Phys. Rev. E* **1998**, *58*, 5081.

(21) Train, C.; Gheorghe, R.; Krstic, V.; Chamoreau, L.-M.; Ovanesyan, N. S.; Rikken, G. L.; Gruselle, M.; Verdaguer, M. Strong magneto-chiral dichroism in enantiopure chiral ferromagnets. *Nat. Mater.* **2008**, *7*, 729−734.

(22) Saito, M.; Ishikawa, K.; Taniguchi, K.; Arima, T. Magnetic control of crystal chirality and the existence of a large magneto-optical dichroism effect in CuB_2O_4. *Phys. Rev. Lett.* **2008**, *101*, 117402.

(23) Christofi, A.; Stefanou, N. Strong magnetochiral dichroism of helical structures of garnet particles. *Opt. Lett.* **2013**, *38*, 4629−4631.

(24) Robbie, K.; Brett, M. Sculptured thin films and glancing angle deposition: growth mechanics and applications. *J. Vac. Sci. Technol. A* **1997**, *15*, 1460−1465.

(25) Hawkeye, M. M.; Brett, M. J. Glancing angle deposition: fabrication, properties, and applications of micro-and nanostructured thin films. *J. Vac. Sci. Technol. A* **2007**, *25*, 1317−1335.

(26) Zhao, Y.-P.; Ye, D.-X.; Wang, G.-C.; Lu, T.-M. Novel nano-column and nano-flower arrays by glancing angle deposition. *Nano Lett.* **2002**, *2*, 351−354.

(27) Gibbs, J. G.; Mark, A. G.; Lee, T.-C.; Eslami, S.; Schamel, D.; Fischer, P. Nanohelices by shadow growth. *Nanoscale* **2014**, *6*, 9457−9466.

(28) Mark, A. G.; Gibbs, J. G.; Lee, T.-C.; Fischer, P. Hybrid nanocolloids with programmed three-dimensional shape and material composition. *Nat. Mater.* **2013**, *12*, 802−807.

(29) Phatak, C.; Liu, Y.; Gulsoy, E. B.; Schmidt, D.; Franke-Schubert, E.; Petford-Long, A. Visualization of the magnetic structure of sculpted three-dimensional cobalt nanospirals. *Nano Lett.* **2014**, *14*, 759−764.

(30) Liu, F.; Umlor, M.; Shen, L.; Weston, J.; Eads, W.; Barnard, J.; Mankey, G. The growth of nanoscale structured iron films by glancing angle deposition. *J. Appl. Phys.* **1999**, *85*, 5486−5488.

(31) Glass, R.; Möller, M.; Spatz, J. P. Block copolymer micelle nanolithography. *Nanotechnology* **2003**, *14*, 1153.

(32) Gibbs, J.; Mark, A.; Eslami, S.; Fischer, P. Plasmonic nanohelix metamaterials with tailorable giant circular dichroism. *Appl. Phys. Lett.* **2013**, *103*, 213101.

(33) Néel, L. Théorie du traînage magnétique des ferromagnétiques en grains fins avec applications aux terres cuites. *Ann. Géophys.* **1949**, *5*, 99−136.

(34) Rikken, G.; Fölling, J.; Wyder, P. Electrical magnetochiral anisotropy. *Phys. Rev. Lett* **2001**, *87*, 236602.

(35) Wagnière, G. H.; Rikken, G. L. Chirality and magnetism: free electron on an infinite helix, NCD, MCD, and magnetochiral dichroism. *Chem. Phys. Lett.* **2009**, *481*, 166−168.

(36) Tellegen, B. D. The gyrator, a new electric network element. *Philips Res. Rep.* **1948**, *3*, 81−101.
(37) Ghosh, A.; Sheridon, N.; Fischer, P. Voltage-controllable magnetic composite based on multifunctional polyethylene microparticles. *Small* **2008**, *4*, 1956−1958.
(38) Wagnière, G. Inverse magnetochiral birefringence. *Phys. Rev. A* **1989**, *40*, 2437.
(39) Temnov, V. V.; Armelles, G.; Woggon, U.; Guzatov, D.; Cebollada, A.; Garcia-Martin, A.; Garcia-Martin, J.-M.; Thomay, T.; Leitenstorfer, A.; Bratschitsch, R. Active magneto-plasmonics in hybrid metal−ferromagnet structures. *Nat. Photonics* **2010**, *4*, 107−111.
(40) Belotelov, V.; Akimov, I.; Pohl, M.; Kotov, V.; Kasture, S.; Vengurlekar, A.; Gopal, A. V.; Yakovlev, D.; Zvezdin, A.; Bayer, M. Enhanced magneto-optical effects in magnetoplasmonic crystals. *Nat. Nanotechnol.* **2011**, *6*, 370−376.
(41) Bonanni, V.; Bonetti, S.; Pakizeh, T.; Pirzadeh, Z.; Chen, J.; Nogués, J.; Vavassori, P.; Hillenbrand, R.; Åkerman, J.; Dmitriev, A. Designer magnetoplasmonics with nickel nanoferromagnets. *Nano Lett.* **2011**, *11*, 5333−5338.
(42) Armelles, G.; Cebollada, A.; García-Martín, A.; García-Martín, J. M.; González, M. U.; González-Díaz, J. B.; Ferreiro-Vila, E.; Torrado, J. Magnetoplasmonic nanostructures: systems supporting both plasmonic and magnetic properties. *J. Opt. A: Pure Appl. Opt.* **2009**, *11*, 114023.